NATURAL CONVECTION FLUID FLOW AND HEAT TRANSFER IN POROUS MEDIA

Elsa Báez and Alfredo Nicolás

NATURAL CONVECTION FLUID FLOW AND HEAT TRANSFER IN POROUS MEDIA

ELSA BÁEZ AND ALFREDO NICOLÁS

Natural convection and heat transfer of fluid flow are studied numerically inside a rectangular cavity with inclination filled with a porous medium. The mass and momentum equations are given by the Darcy equations coupled with the thermal energy equation through the unsteady Boussinesq approximation. The two-dimensional restriction in terms of the stream function and vorticity variables is considered. The study is analyzed in terms of several values of the parameters that determine the evolution of the flow: the Rayleigh Number, the aspect ratio of the cavity and the angle of inclination.

1. Introduction

The mass and momentum equations in natural convection fluid flow in a porous medium are given by the Darcy equations coupled with the thermal energy equation through the unsteady Boussinesq approximation to deal with an incompressible structure. In this work the dimensionless problem is formulated in terms of the stream function and vorticity variables; then, the computation of the pressure is avoided and the incompressibility condition is satisfied automatically. Regarding the numerical method, once a convenient second order time discretization is performed, a nonlinear elliptic system is obtained which is solved through a fixed point iterative process. The iterative process leads to the solution of uncoupled, well-conditioned, symmetric linear elliptic problems for which very efficient solvers exist regardless of the space discretization.

The study of natural convection and heat transfer of fluid flow in a porous medium has important technological applications: storage and preservation of grains and cereals; solar energy collectors; filter systems; transport of radioactive wastes through the soil; and postaccident heat removal in nuclear reactors. Our numerical study is carried out on tilted rectangular cavities. The study is realized through the parameters that influence directly the behavior and evolution of the flow: the Rayleigh Number Ra, the aspect ratio of the cavity A, and the angle of inclination ϕ.

We mention below two categories of research in connection with natural convection problems that arise when opposing walls of a cavity are subjected to a temperature gradient and where the other set of walls is insulated—the subject of the present work.

(i) The steady problem: Vasseur et al. [1987] studied analytically and numerically the flow in a tilted rectangular cavity and observed that the maximum heat transfer, for a given Ra, is obtained when the cavity is heated from below, with ϕ in the range $90° < \phi < 180°$. They found that this maximum takes place for values of ϕ approaching $90°$ whenever Ra increases. Moya et al. [1987] studied the problem in tilted horizontal rectangular cavities for Rayleigh number Ra $= 100$ and found

multiple cellular flow. Sen et al. [1987] studied the multiplicity of solutions, considering vertical and horizontal inclined cavities, and showed analytical and numerical results for Rayleigh numbers Ra $\leq$ 500 with small angles.

(ii) The unsteady problem : Baytas [2000] showed results in a tilted square cavity for Rayleigh numbers 10^2, 10^3, and 10^4. Saeid and Pop [2004] studied the transient evolution for Rayleigh numbers with values of $10^2 - 10^4$ in a square cavity, and reported the final time when the steady state is reached.

Results for Ra $= 10^2$ and 10^3 are reported to validate the numerical method; these flows, obtained from the unsteady problem, agree with the ones obtained by other authors solving either the steady problem or the unsteady one but using different methods. Results for Ra $\geq 10^2$ with $A = 4$ and 8 are also reported, which to the best of our knowledge, have not been presented before. To assure that these new flows are correct, a time step and mesh independence studies have been made. All the results are complemented with their local and global Nusselt numbers on the hot wall, and the extreme values of the stream function. Actually, results with the numerical method described here are reported in [Báez and Nicolás 2006], where the numerical method is extended to include natural convection flows in homogeneous fluids (the evolution of some oscillatory, time-dependent, flows is also described therein); however, the results for porous media reported here are different from those shown in that work.

2. Mathematical models

Nomenclature

W	width of the cavity
H	height of the cavity
A	aspect ratio of the cavity $(=H/W)$
ρ	density
ρ_0	reference density
T	temperature
T_r	reference temperature
β	thermal expansion coefficient
k	permeability of porous medium
η	thermal diffusivity
μ	dynamic viscosity
ν	kinematic viscosity $(=\frac{\mu}{\rho_0})$
t	dimensionless time
u	dimensionless velocity vector ($\mathbf{u} = (u_1, u_2)$)
p	dimensionless pressure
θ	dimensionless temperature
ψ	stream function
Ra	Rayleigh number
ϕ	angle of inclination of the cavity
g	gravity constant
e	unitary vector in the gravity direction

Nu   local Nusselt number
$\overline{\text{Nu}}$ global Nusselt number

Natural convection flow of a thermal viscous fluid assumed to be Newtonian is considered under the well known Boussinesq approximation in the presence of a gravitational field. Let $\Omega \subset R^N$ ($N = 2, 3$) be the region of the flow of an unsteady, viscous, and thermal fluid, and Γ the boundary of the region. This kind of flow may be governed by the following dimensionless system of equations with incompressible structure:

$$
\begin{cases}
t > 0: \\
\mathbf{u} + \nabla p = \text{Ra}\,\theta \mathbf{e}, & \text{in } \Omega, \quad \text{(a)} \\
\nabla \cdot \mathbf{u} = 0, & \text{in } \Omega, \quad \text{(b)} \\
\theta_t - \nabla^2 \theta + \mathbf{u} \cdot \nabla \theta = 0, & \text{in } \Omega. \quad \text{(c)}
\end{cases}
\tag{1}
$$

Equations (1)a–b are the Darcy equations in primitive variables $\mathbf{u}$ and p coupled with the temperature Equation (1)c; Equation (1)b is known as the *incompressibility condition*. The Rayleigh number is given by

$$
\text{Ra} = \frac{k\beta L g (T_h - T_c)}{\eta \nu},
$$

with T_h as the constant temperature on the hot wall, T_c that of the cold wall, and L as a reference length. The system must be supplemented with initial conditions $\mathbf{u}(\mathbf{x}, 0) = \mathbf{u}_0(\mathbf{x})$ and $\theta(\mathbf{x}, 0) = \theta_0(\mathbf{x})$ in Ω, and boundary conditions: for instance $\mathbf{u} = \mathbf{f}$ and $B\theta = 0$ on Γ, $t \geq 0$, where B is a temperature boundary operator that can involve Dirichlet, Neumann or mixed boundary conditions. Figure 1 shows the geometry of the model considered.

Restricting the system in Equation (1) to a two-dimensional region Ω, applying the rotational in both sides of the momentum equation, and considering that $\nabla \cdot \mathbf{u} = 0$, imply the existence of a function ψ, called the stream function, such that

$$
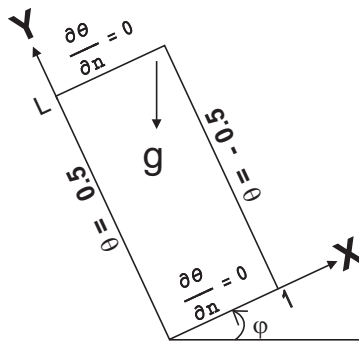u_1 = \frac{\partial \psi}{\partial y}, \quad u_2 = -\frac{\partial \psi}{\partial x},
\tag{2}
$$

Figure 1. Geometry of the model.

the following scalar system is then obtained, where the unitary vector **e** has been replaced by the contribution of the angle of inclination ϕ of the region Ω through $\mathbf{e} = (\sin\phi, \cos\phi)$:

$$\begin{cases} t > 0: \\ -\nabla^2\psi = \text{Ra}\left(\frac{\partial\theta}{\partial x}\cos\phi - \frac{\partial\theta}{\partial y}\sin\phi\right), & \text{in } \Omega, \\ \theta_t - \nabla^2\theta + \mathbf{u}\cdot\nabla\theta = 0, & \text{in } \Omega. \end{cases} \tag{3}$$

This system represents the Boussinesq approximation in stream-function vorticity variables of system Equation (1) in primitive variables. As pointed out in Section 1, the pressure has been eliminated since the curl of the gradient is zero and the incompressibility condition is satisfied automatically by Equation (2). This work is concerned with natural convection in rectangular cavities, and so the equations are set in $\Omega = (0, W) \times (0, H)$. For viscous fluids $\mathbf{u} = \mathbf{0}$ on solid and fixed walls, all the walls of the cavities are solid and fixed in natural convection, and so, by Equation (2), ψ is constant and this constant can be chosen to be 0.

The local Nusselt number Nu measures the heat transfer at each point on the hot wall where the temperature is specified, and the global Nusselt number $\overline{\text{Nu}}$ measures the total rate of heat transfer on the same wall. These nondimensional parameters are defined by

$$\text{local Nusselt number:} \quad \text{Nu}(y) = A|\frac{\partial\theta}{\partial x}||_{x=0};$$

$$\text{global Nusselt number:} \quad \overline{\text{Nu}} = \int_0^H \text{Nu}(y)\,dy.$$

3. Numerical scheme

The time derivative θ_t in the system of Equation (3) is approximated by

$$f_t\big(\mathbf{x}, (n+1)\Delta t\big) \approx \frac{1.5f^{n+1} - 2f^n + 0.5f^{n-1}}{\Delta t}, \qquad n \geq 1, \quad \mathbf{x} \in \Omega, \tag{4}$$

where $\Delta t > 0$ is the time discretization step, f^r is an approximation of $f(x, r\Delta t)$, and where it is known that Equation (4) is a second order approximation for sufficiently smooth function f.

Then, once Equation (4) is applied to θ_t the following nonlinear elliptic system is obtained, incorporating the boundary condition for ψ and θ as discussed before:

$$\begin{cases} -\nabla^2\psi^{n+1} = \text{Ra}(\frac{\partial\theta^{n+1}}{\partial x}\cos\phi - \frac{\partial\theta^{n+1}}{\partial y}\sin\phi) & \text{in } \Omega, \quad \psi^{n+1} = 0 \quad \text{on } \Gamma, \\ \alpha\theta^{n+1} - \nabla^2\theta^{n+1} + \mathbf{u}^{n+1}\cdot\nabla\theta^{n+1} = f_\theta & \text{in } \Omega, \quad B\theta^{n+1} = 0 \quad \text{on } \Gamma, \end{cases} \tag{5}$$

where $\alpha = \frac{1.5}{\Delta t}$, $f_\theta = \frac{2\theta^n - 0.5\theta^{n-1}}{\Delta t}$, $\mathbf{u}$ in terms of ψ is given by Equation (2), and B is still the temperature boundary operator.

Renaming $(\psi^{n+1}, \theta^{n+1})$ by (ψ, θ) to simplify the notation, we must solve at each time level, for Equation (5), a nonlinear elliptic system of the form

$$\begin{cases} -\nabla^2\psi = Ra(\frac{\partial\theta}{\partial x}\cos\phi - \frac{\partial\theta}{\partial y}\sin\phi) & \text{in } \Omega, \quad \psi = 0 \quad \text{on } \Gamma \\ \alpha\theta - \nabla^2\theta + \mathbf{u}\cdot\nabla\theta = f_\theta & \text{in } \Omega, \quad B\theta = 0 \quad \text{on } \Gamma. \end{cases} \tag{6}$$

To obtain (ψ^1, θ^1) in Equation (5), a first order approximation is applied to the temporal derivative with a smaller time step to maintain second order precision; an elliptic system like the one in Equation (6) is also obtained.

Given

$$\Theta(\psi, \theta) \equiv (\alpha I - \nabla^2 \theta) + \mathbf{u} \cdot \nabla \theta - f_\theta \text{ in } \Omega,$$

then system Equation (6) is equivalent to

$$\begin{cases} -\nabla^2 \psi = \text{Ra}(\frac{\partial \theta}{\partial x} \cos \phi - \frac{\partial \theta}{\partial y} \sin \phi) & \text{in } \Omega, \quad \psi|_\Gamma = 0, \\ \Theta(\psi, \theta) = 0 & \text{in } \Omega, \quad B\theta|_\Gamma = 0. \end{cases} \tag{7}$$

System Equation (7) is solved with the following fixed point iterative process:

$$\begin{cases} \text{Knowing } \theta^0 = \theta^n \text{ solve until convergence on } \theta \\ -\nabla^2 \psi^{m+1} = \text{Ra}(\frac{\partial \theta^m}{\partial x} \cos \phi - \frac{\partial \theta^m}{\partial y} \sin \phi) & \text{in } \Omega, \quad \psi^{m+1} = 0 \quad \text{on } \Gamma, \quad \text{(a)} \\ \theta^{m+1} = \theta^m - \lambda(\alpha I - \nabla)^{-1}\Theta(\psi^{m+1}, \theta^m) & \text{in } \Omega, \quad B\theta^{m+1} = 0 \quad \text{on } \Gamma, \lambda > 0, \quad \text{(b)} \\ \text{and take } (\psi^{n+1}, \theta^{n+1}) = (\psi^{m+1}, \theta^{m+1}). \end{cases} \tag{8}$$

The partial differential equation problem for θ^{m+1} in Equation (8)b is equivalent to

$$(\alpha I - \nabla^2)\theta^{m+1} = (\alpha I - \nabla^2)\theta^m - \lambda\Theta(\psi^{m+1}, \theta^m) \quad \text{in } \Omega, \quad B\theta^{m+1}|_\Gamma = 0.$$

Therefore, at each iteration of each time level, uncoupled, well-conditioned, symmetric elliptic linear problems associated with the operators $-\nabla^2$ and $\alpha I - \nabla^2$ must be solved.

For linear elliptic problems, very efficient solvers exist regardless of the space discretization. The results in this work are obtained with the second-order approximation of the Fishpack solver [Adams et al. 1980], where the algebraic linear systems are solved with an efficient cyclic reduction iterative method [Sweet 1977]. As mentioned before, the first time derivative θ_t is approximated by Equation (4), which is a second-order approximation, whereas the first space derivatives of ψ in Equation (2) to obtain $\mathbf{u}$ in Equation (6), the normal derivative of the boundary condition for θ (described later), and the first space derivative for the local Nusselt number are approximated by the centered second-order finite difference approximation in interior points and by Equation (4) in boundary points. To approximate the integral in the global Nusselt number the second-order trapezoid rule (in the entire interval) is used. All these kinds of approximations imply that the whole discrete problem relies on second-order approximations.

4. Numerical results

The initial condition for the temperature is given by $\theta(\mathbf{x}, 0) = 0$. The discretization parameters, time step Δt and the size of the mesh $h_x \times h_y$, will be specified in each case under study. In the iterative process, the parameter λ is chosen as $\lambda = 0.7$ and the stopping absolute criterion as 10^{-5}.

The results are reported through the streamlines of the stream function and the isotherms of the temperature; most of the isocontours are specified for each case, otherwise they are the default ones. All the results are also complemented with their local Nu and global $\overline{\text{Nu}}$ Nusselt numbers, in order to see the local and global heat transfer, as well as the extreme values of the stream function ψ.

The results shown correspond to steady state flows from the unsteady problem. They are the converged asymptotic steady state as time t approaches $+\infty$ (large time, in practice). To reach convergence to an asymptotic steady state a stopping criterion must be given for the final time T_{ss} when it occurs. Since T_{ss} is the time when the solution does not change any more with respect to time at any spatial point occupied by the fluid [Nicolás and Bermúdez 2005], T_{ss} is determined with the point-wise discrete L_∞ absolute criterion in the closure $\overline{\Omega}$ of the cavity

$$\theta : \ ||\theta_{hx,hy}^{n+1} - \theta_{hx,hy}^n||_\infty,$$

with tolerance 10^{-5}. For $\text{Ra} = 10^2$ and $\text{Ra} = 10^3$ results are shown to validate the numerical method mainly in the square cavity with results other authors have obtained solving the steady problem or the unsteady one but using a different method. New results, to the best of our knowledge reported here for the first time, are presented for $\text{Ra} \geq 10^2$ with aspect ratios $A = 4, \ 8$. To support the validity of these results, a time step and mesh independence studies have been made with the point-wise discrete L_∞ relative error in $\overline{\Omega}$

$$\begin{cases} \Delta t \text{ fixed}: & \dfrac{||f_{hx1,hy1;\Delta t} - f_{hx2,hy2;\Delta t}||_\infty}{||f_{hx1,hy1;\Delta t}||_\infty}, \\[2ex] \{h_x, h_y\} \text{ fixed}: & \dfrac{||f_{hx,hy;\Delta t1} - f_{hx,hy;\Delta t2}||_\infty}{||f_{hx,hy;\Delta t1}||_\infty}. \end{cases}$$

The specific temperature boundary condition to be considered, described so far in the boundary operator B, is given by

$$\frac{\partial \theta}{\partial y} = 0 \quad \text{on } \Gamma|_{y=0,W}, \qquad \theta = 0.5 \quad \text{on } \Gamma|_{x=0}, \qquad \theta = -0.5 \quad \text{on } \Gamma|_{x=1};$$

that is, horizontal walls are adiabatic and the hot and cold wall are the left and the right wall, respectively.

Figure 2 shows the streamlines and isotherms for $\text{Ra} = 10^2$ in the unit square, that is $A = 1$, and $0° \leq \phi \leq 90°$. This range of angles means that heating from the lateral (left) wall to heating on the bottom wall is considered.

It is observed from the streamlines of Figure 2 that one main cell only is obtained for the range of angles considered and therefore, from the local Nusselt number graphic, one maximum is also obtained for heat transfer. In this case, from $\psi_{\min}$, it follows that the fluid motion is slower when the heating comes either from the lateral or bottom wall, that is when $\phi = 0°$ or $\phi = 90°$, than for the other angles. It is also observed, from $\overline{\text{Nu}}$ in Figure 1, that the heat transfer is smaller for these angles than for the others.

Figure 3 shows the results for $\text{Ra} = 10^3$ and some angles $0° \leq \phi \leq 360°$ in the unit square cavity also. For $\phi = 0°$, it is observed that the fluid is heated along the left wall causing the less dense fluid to rise toward the top wall; this fluid is then cooled on the right wall, becomes denser, and then falls to the bottom of the cavity, originating a rotating clockwise cell in the streamlines. A similar situation occurs for $40°$ and $330°$; however, the opposite effect occurs for $130°$. In this case, the main cell rotates counterclockwise since the hot wall is below the cold one and the isotherms show that the hot fluid is localized toward the top of the right part of the tilted cavity while the cold fluid resides toward the bottom of the left part. Secondary cells appear for some angles, for instance $\phi = 330°$. The graphic of the local Nusselt number shows that the maximum value for $0°$, $40°$, and $330°$ is reached on the bottom wall
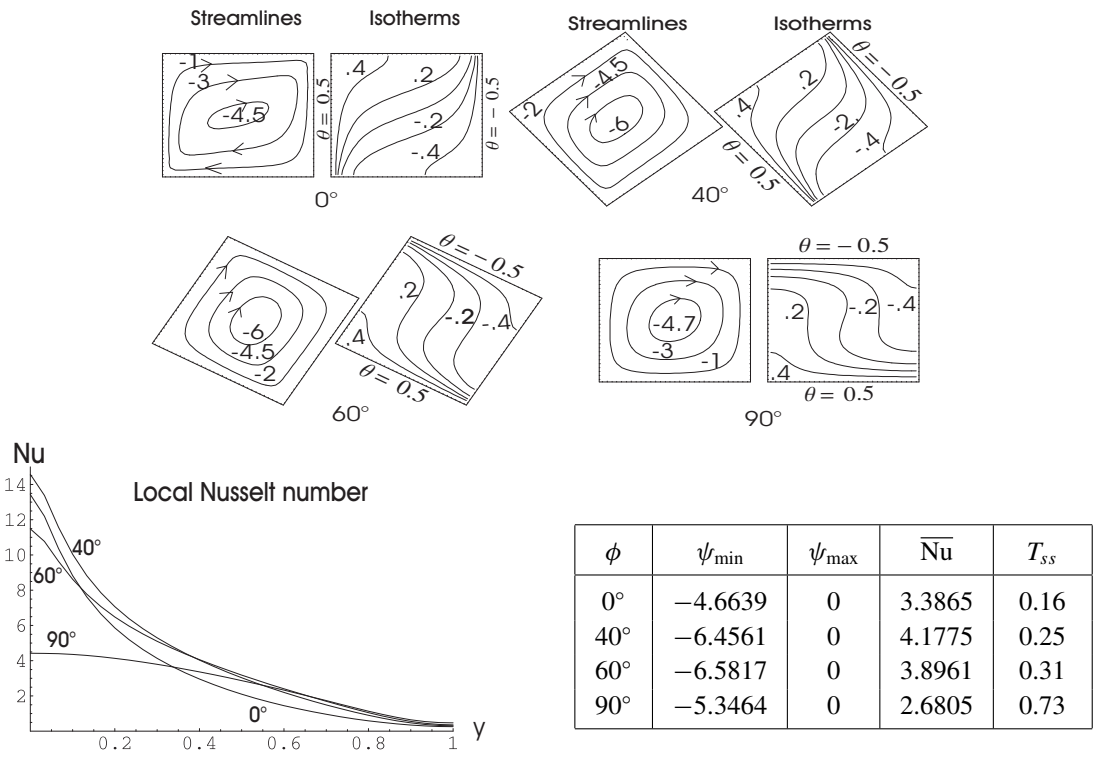
Figure 2. Results for $Ra = 10^2$, $A = 1$, $\Delta t = 10^{-2}$ and $h_x \times h_y = \frac{1}{30} \times \frac{1}{30}$.

ϕ	$\psi_{\min}$	$\psi_{\max}$	$\overline{Nu}$	T_{ss}
0°	−4.6639	0	3.3865	0.16
40°	−6.4561	0	4.1775	0.25
60°	−6.5817	0	3.8961	0.31
90°	−5.3464	0	2.6805	0.73

whereas for 130° the opposite occurs, that is, the maximum is reached on the top wall because of the buoyancy effect.

The corresponding results for the minimum and maximum values of the stream function, $\psi_{\min}$ and $\psi_{\max}$, the global Nusselt number $\overline{Nu}$, and the final time T_{ss} when the flow reaches the steady state are displayed in Figure 3. The extreme values of the stream function indicate an increase in the fluid motion for the angles $\phi = 40°$ and $\phi = 130°$, implying an increase of heat transfer, because of $\overline{Nu}$, although this is higher for the first angle than for the second, whereas for 330° less fluid motion is obtained implying a diminution of the heat transfer.

The above results for $Ra = 10^2$ and $Ra = 10^3$ as well as others obtained for $Ra = 10^2$ and $Ra = 10^4$ with $0° \leq \phi \leq 360°$ are in agreement with those reported in [Baytas 2000] from the unsteady problem also but using a different method. For these three values of Ra one main cell is obtained for almost all values of ϕ and secondary cells appear for some angles when $Ra = 10^3$ and 10^4, as pointed out before for $Ra = 10^3$.

As already mentioned, the new results are shown for values of Rayleigh number $Ra \geq 10^2$ with aspect ratios $A \geq 1$. For $Ra = 10^2$ and the aspect ratio is augmented to $A = 4$, it can be seen in Figure 4 that there appears from one cell for $\phi = 0°$ to five cells when the cavity is heated on the bottom, that is for $\phi = 90°$. The local Nusselt number graphic shows one maximum for $\phi = 0°$ and $\phi = 58°$, two for $\phi = 65°$ and three for $\phi = 90°$.
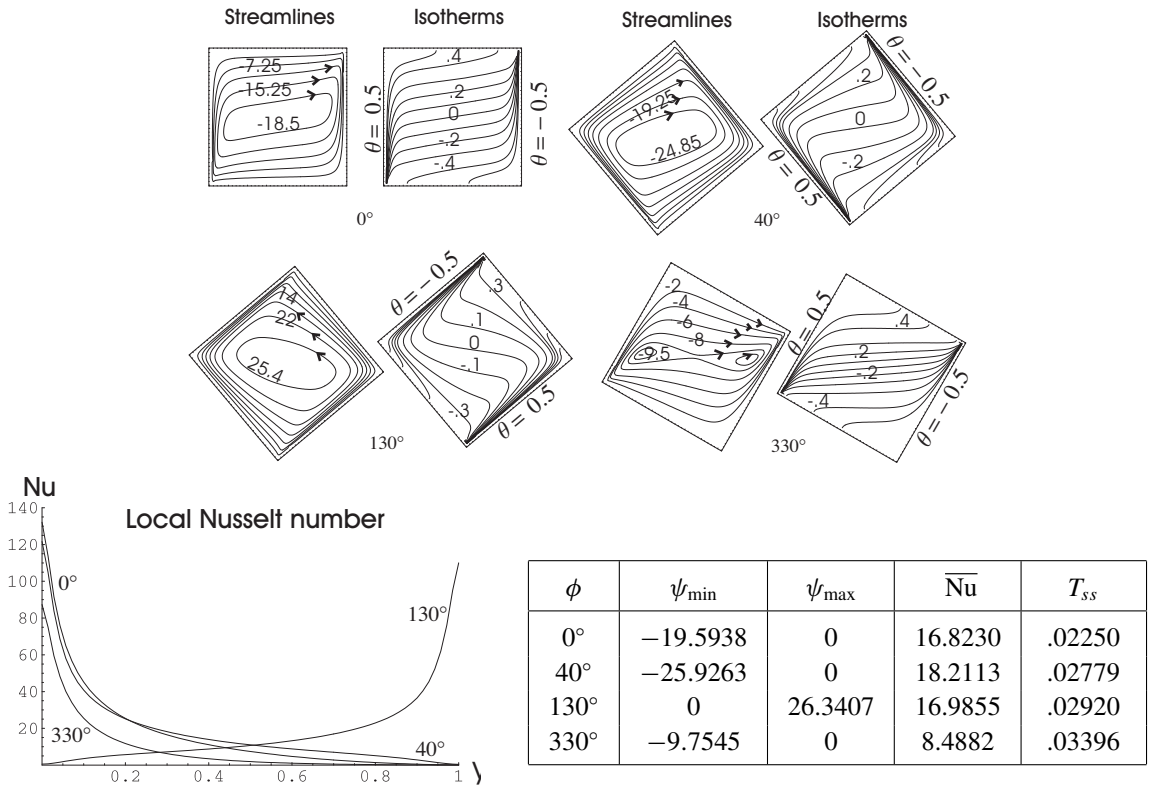
Figure 3. Results for Ra $= 10^3$, $A = 1$, $\Delta t = 10^{-5}$ and $h_x \times h_y = \frac{1}{70} \times \frac{1}{70}$.

ϕ	$\psi_{\min}$	$\psi_{\max}$	$\overline{\text{Nu}}$	T_{ss}
0°	−19.5938	0	16.8230	.02250
40°	−25.9263	0	18.2113	.02779
130°	0	26.3407	16.9855	.02920
330°	−9.7545	0	8.4882	.03396

Figure 4 indicates that the fluid motion is faster when the cavity is heated laterally, $\phi = 0°$, than when it is heated from below, $\phi = 90°$; however, the heat transfer is larger when three cells appear, $\phi = 65°$.

Figure 5 shows that when Ra $= 10^2$ and $A = 8$, the fluid motion ranges from one cell rotating clockwise for $\phi = 0°$ (lateral heating) to eleven cells circulating in directions opposite to one another for $\phi = 90°$ (heating on the bottom). The local Nusselt number graphic shows one maximum when one main cell appears, 0°; a similar situation occurs for 50°, whereas for $\phi = 70°$, there exist five maxima and six for 90°, indicating that there are several places on the hot wall where the heat transfer is increased: those between cells where the fluid moves from the cold to the hot wall. The minima correspond to flow moving in opposite directions.

From the extremum values of the stream function in Figure 5, it follows that the fluid motion is stronger when $\phi = 0°$ than when $\phi = 90°$, but this is not reflected on the global heat transfer coefficient, $\overline{\text{Nu}}$: a high heat transfer is given for those angles when multiple cells appear. However, from other experiments for Ra $= 10^2$ and Ra $= 10^3$ with $A > 1$, when plotting $\overline{\text{Nu}}$ versus ϕ, was observed that one maximum of $\overline{\text{Nu}}$ is obtained for those angles ϕ with a single cell and a second maximum appears for those angles with multiple cells.
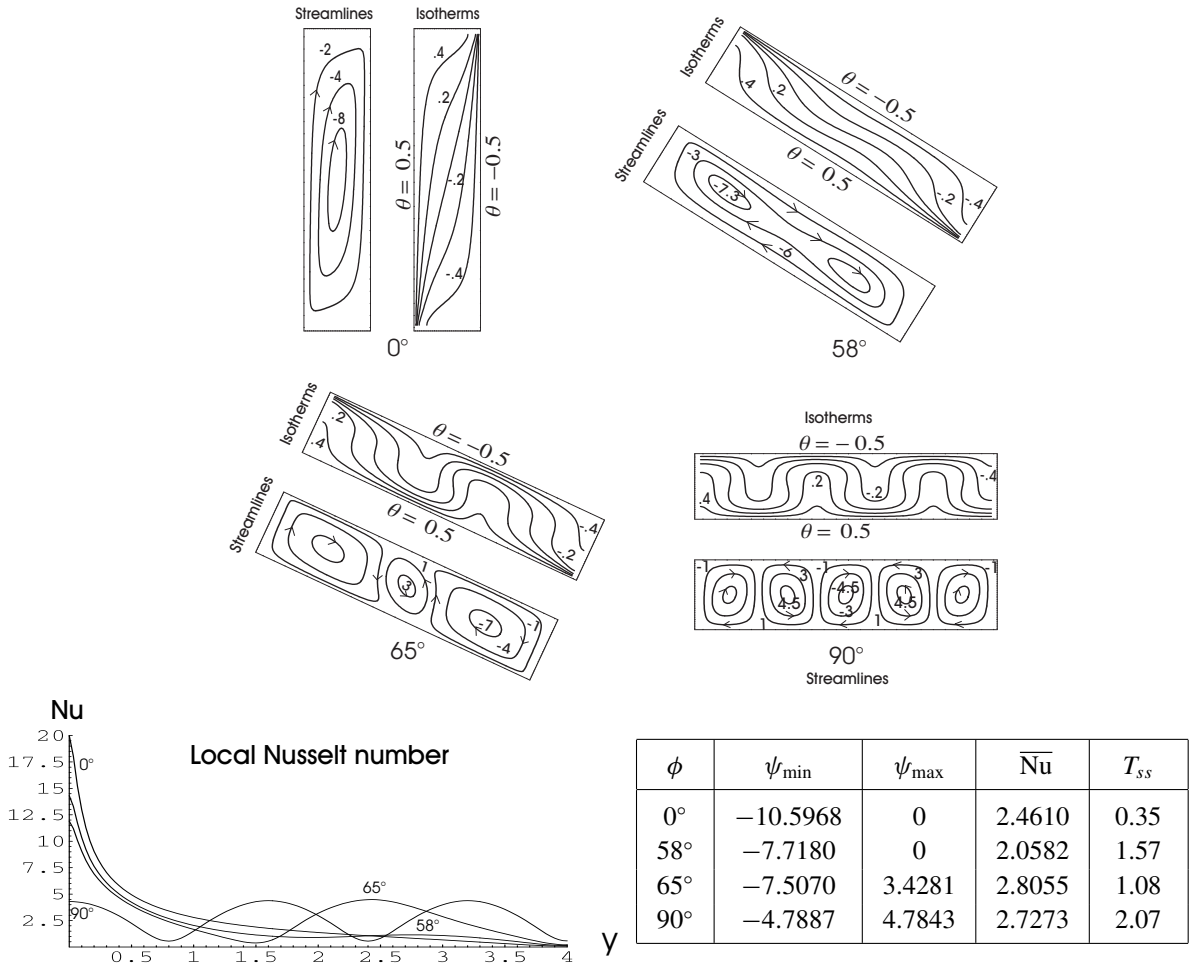
Figure 4. Results for $\mathrm{Ra} = 10^2$, $A = 4$, $\Delta t = 10^{-2}$ and $h_x \times h_y = \frac{1}{30} \times \frac{4}{120}$.

To demonstrate that the flows in Figures 4 and 5 are correct, a time step and mesh independence studies were performed in the vertical case, $\phi = 0°$, with $A = 8$ in Figure 5, for three mesh sizes and three times as follows:

(1) time step fixed, $\Delta t = 10^{-2}$ and $(h_x, h_y) = (1/30, 8/240)$, $(1/45, 8/360)$, $(1/60, 8/480)$;

(2) mesh size fixed $(h_x, h_y) = (1/30, 1/240)$ and $\Delta t = 10^{-2}$, 5×10^{-3}, 2.5×10^{-3}.

The respective discrepancies are:

(1) less than $6 \times 10^{-2}\%$ (at most $3.8 \times 10^{-1}\%$ for stream function and $5.9 \times 10^{-1}\%$ for temperature);

(2) at most $4.96 \times 10^{-2}\%$ ($2.44 \times 10^{-2}\%$ for stream function and $4.96 \times 10^{-2}\%$ for temperature).

The corresponding minima of the stream function ψ in each case (the maximum value is always zero) are:
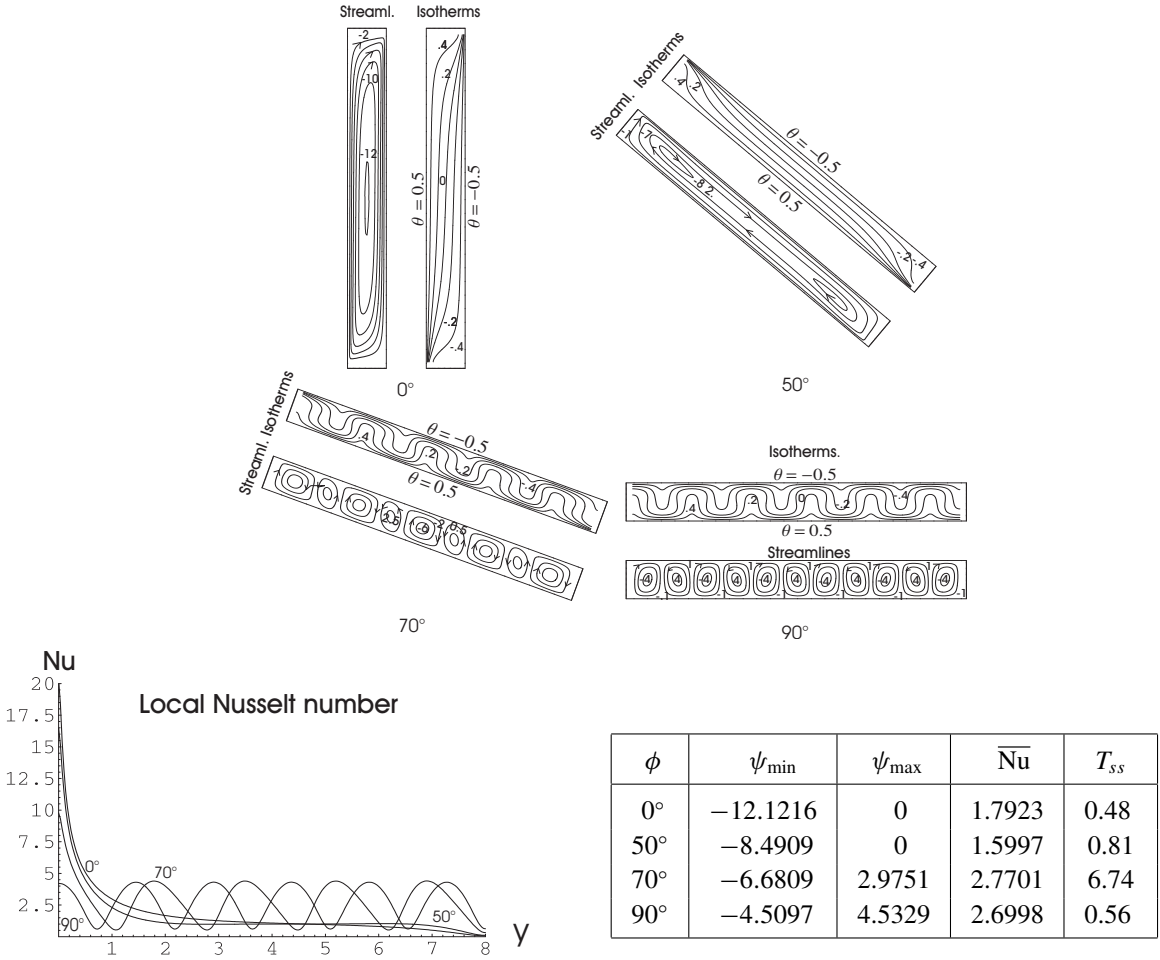
Figure 5. Results for $\mathrm{Ra} = 10^2$, $A = 8$, $\Delta t = 10^{-2}$ and $h_x \times h_y = \frac{1}{30} \times \frac{8}{240}$.

(1) min $= -12.1216$, -12.1206, -12.1280, respectively;

(2) min $= -12.1216$, -12.1223, -12.1238, respectively.

Therefore, the results shown in Figure 5 are chosen as the correct ones.

For the corresponding easier case with $A = 4$ in Figure 4 something similar occurs.

In Figure 6, results for $\mathrm{Ra} = 10^3$ and some angles $0°leq\phi \leq 360°$ with $A = 4$ are presented. A single large cell appears for angles $\phi = 0°$ and $\phi = 65°$ rotating clockwise. Experiments show that multiple cells appear for angles $66° \leq \phi \leq 114°$, the result for $\phi = 110°$ is an example of this situation: seven main cells appear, five small cells occupying the middle of the cavity enclosed by two big ones in the extremes of the cavity and rotating in opposite direction each other. The graphic of the local Nusselt number shows that the maximum heat transfer for this angle is localized on the top of the cavity due to the reverse effect of the buoyancy force, in comparison to the other angles; the other maximums are a consequence of the fact that multiple cells appear.
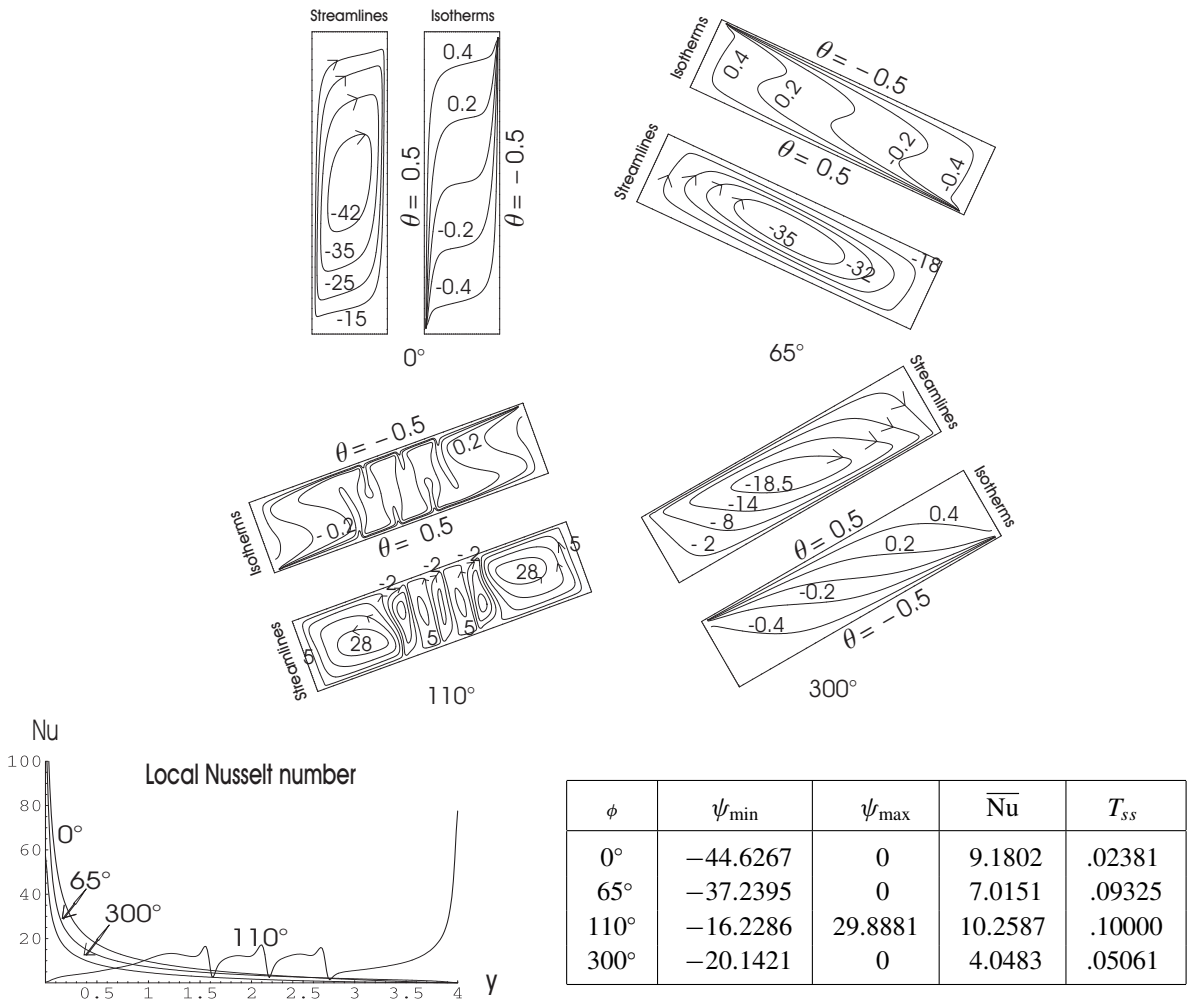
ϕ	$\psi_{\min}$	$\psi_{\max}$	$\overline{\mathrm{Nu}}$	T_{ss}
0°	−44.6267	0	9.1802	.02381
65°	−37.2395	0	7.0151	.09325
110°	−16.2286	29.8881	10.2587	.10000
300°	−20.1421	0	4.0483	.05061

Figure 6. Results for $\mathrm{Ra} = 10^3$, $A = 4$, $\Delta t = 10^{-5}$ and $h_x \times h_y = \frac{1}{70} \times \frac{4}{280}$.

From Figure 6 it is also observed that a stronger fluid motion occurs for 0° than for 110°; however, the corresponding value of the global Nusselt number for 0°, when there is a single cell, indicates a smaller heat transfer than for 110°, when multiple cells appear.

Figure 7 pictures numerical results for the same Rayleigh number with $A = 8$ and several angles $0° \le \phi \le 360°$. Multiple cells may appear for some angles, as shown for $\phi = 117°$, which indicate a more complex fluid motion. On the other hand, Figure 5 shows that with some angles the fluid motion is stronger than others, but the corresponding value of the heat transfer is smaller. Complemented with other experiments, not shown here, it may be concluded that this situation is characteristic of aspect ratios $A > 1$.
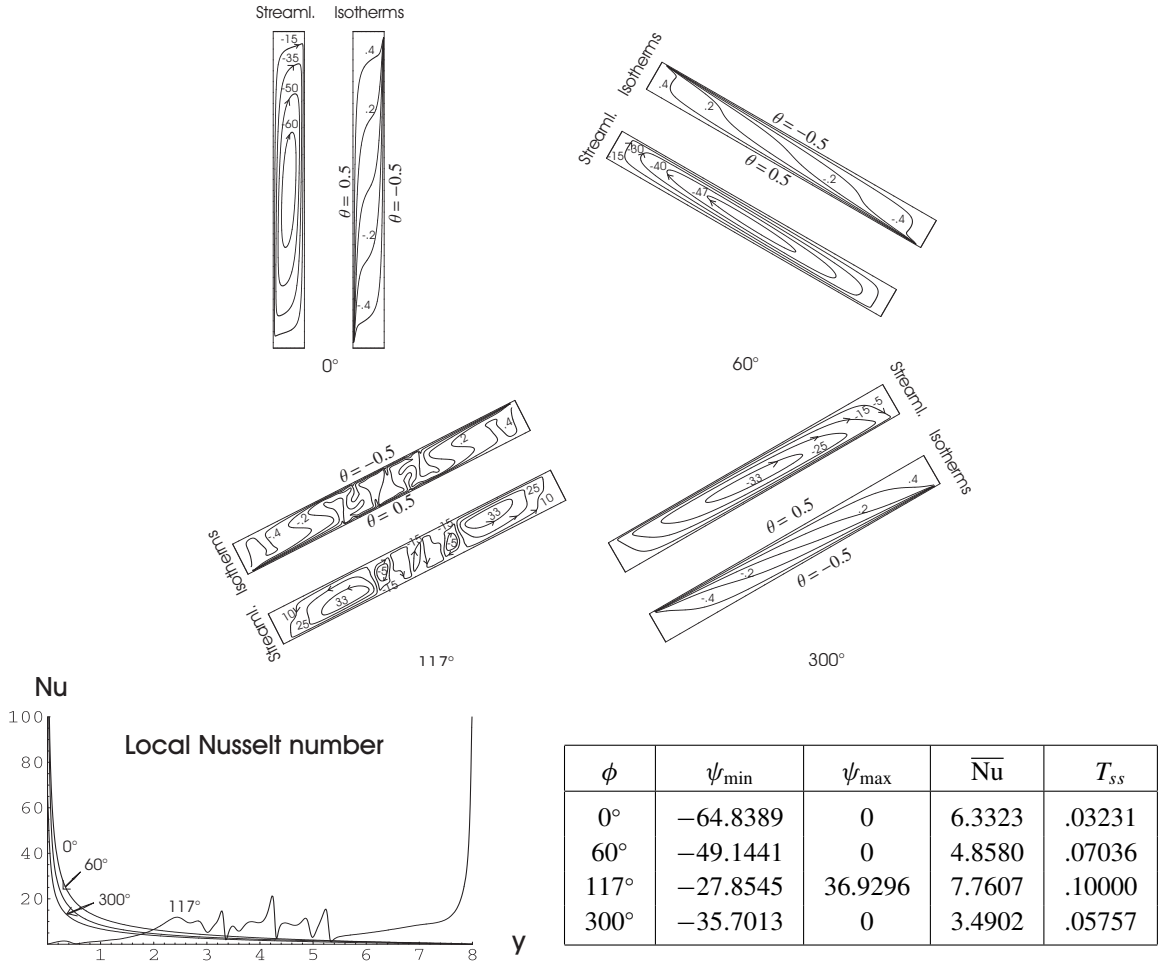
Figure 7. Results for $\mathrm{Ra} = 10^3$, $A = 8$, $\Delta t = 10^{-5}$ and $h_x \times h_y = \frac{1}{70} \times \frac{8}{560}$.

To show that the flows in Figures 6 and 7 are correct, a time step and mesh independence studies were performed in the vertical case, $\phi = 0°$, with $A = 8$ in Figure 7, for three mesh sizes and three times as follows:

(1) time step fixed, $\Delta t = 10^{-5}$ and $(h_x, h_y) = (1/70,\ 8/560),\ (1/105,\ 8/840),\ (1/140,\ 8/1120)$;

(2) mesh size fixed $(h_x, h_y) = (1/70, 8/560)$ and $\Delta t = 10^{-5},\ 5 \times 10^{-6},\ 2.5 \times 10^{-6}$.

The respective discrepancies are:

(1) less than 2% (at most 1.67% for stream function and 1.59% for temperature);

(2) at most 5.16% (5.16% for stream function and 2.15% for temperature).

The corresponding minima of the stream function ψ in each case (the maximum value is always zero) are:

(1) min = $-64.8389,\ -64.8197,\ -64.8379$, respectively;

(2) min $= -64.8389, -64.8415, -64.8351$, respectively.

Therefore, the results shown in Figure 7 are chosen as the correct ones.

For the corresponding easier case with $A = 4$ in Figure 6 something similar occurs.

5. Conclusions

From the numerical experiments we observe that when Ra increases, the time step and the spatial mesh size must necessarily be significantly diminished—which can become a problem computationally speaking, at least in the current form of the numerical method. The results obtained for several values of the Rayleigh number, the aspect ratio, and the angle of inclination of the cavity indicate that the flow is affected whenever the value of each of these parameters changes. The fluid motion is strong not only when Ra increases but also when A increases and Ra is fixed. The global Nusselt number shows also that the heat transfer increases as Ra increases, but when this value is fixed and the aspect ratio is larger, the heat transfer is smaller. For angles where multiple cells appear the global heat transfer is higher than for those with a single cell. Moreover, there exist two maxima of the global heat transfer, as a function of the angle ϕ, with $0° \leq \phi \leq 90°$: one for angles when a single cell appears and one more for angles with multiple cells. About the time T_{ss} necessary to reach a steady state, for ϕ fixed, it can be observed that T_{ss} is smaller whenever Ra is higher; however, this time increases whenever A increases. It may be pointed out that with some modifications of the numerical method, the case with variable porosity [Marcondes et al. 2001] and variable anisotropy [Nguyen et al. 1994] can be also explored as well as viscous effects near walls through the Brinkman extension [Rees 1999].

Acknowledgements

References

[Adams et al. 1980] J. Adams, P. Swarztrauber, and R. Sweet, "FISHPACK: a package of Fortran subprograms for the solution of separable elliptic PDE's", technical report, The National Center for Atmospheric Research, Boulder, CO, 1980.

[Báez and Nicolás 2006] E. Báez and A. Nicolás, "2D natural convection flows in tilted cavities: porous media and homogeneous fluids", *Int. J. Heat Mass Tran.* **49**:25-26 (2006), 4773–4785.

[Baytas 2000] A. C. Baytas, "Entropy generation for natural convection in an inclined porous cavity", *Int. J. Heat Mass Tran.* **43**:12 (2000), 2089–2099.

[Marcondes et al. 2001] F. Marcondes, J. M. De Medeiros, and J. M. Gurgel, "Numerical analysis of natural convection in cavities with variable porosity", *Numer. Heat Tr. A Appl.* **40**:4 (2001), 403–420.

[Moya et al. 1987] S. L. Moya, E. Ramos, and M. Sen, "Numerical study of natural convection in a tilted rectangular porous material", *Int. J. Heat Mass Tran.* **30**:4 (1987), 741–756.

[Nguyen et al. 1994] H. D. Nguyen, S. Paik, and R. W. Douglass, "Study of double-diffusive convection in layered anisotropic porous media", *Numer. Heat Tr. B Fund.* **26**:4 (1994), 489–505.

[Nicolás and Bermúdez 2005] A. Nicolás and B. Bermúdez, "2D thermal/isothermal incompressible viscous flows", *Int. J. Numer. Meth. Fl.* **48**:4 (2005), 349–366.

[Rees 1999] D. A. S. Rees, "Darcy-Brinkman free convection from a heated horizontal surface", *Numer. Heat Tr. A Appl.* **35**:2 (1999), 191–204.

[Saeid and Pop 2004] N. H. Saeid and I. Pop, "Transient free convection in a square cavity filled with a porous medium", *Int. J. Heat Mass Tran.* **47**:8-9 (2004), 1917–1924.

[Sen et al. 1987] M. Sen, P. Vasseur, and L. Robillard, "Multiple steady states for unicellular natural convection in an inclined porous layer", *Int. J. Heat Mass Tran.* **30**:10 (1987), 2097–2113.

[Sweet 1977] R. Sweet, "A cyclic reduction algorithm for solving block tridiagonal systems of arbitrary dimension", *SIAM J. Numer. Anal.* **14**:4 (1977), 706–720.

[Vasseur et al. 1987] P. Vasseur, M. G. Satish, and L. Robillard, "Natural convection in a thin, inclined, porous layer exposed to a constant heat flux", *Int. J. Heat Mass Tran.* **30**:3 (1987), 537–549.

ELSA BÁEZ: ebj@xanum.uam.mx
Depto. Matemáticas, Ed. AT-Diego Bricio, UAM-I, 09340 Mexico D.F., Mexico

ALFREDO NICOLÁS: anc@xanum.uam.mx
Depto. Matemáticas, Ed. AT-Diego Bricio, UAM-I, 09340 Mexico D.F., Mexico